

Hydrogen bond relaxation dynamics of frozen H₂O under compression

Xi Zhang,¹ Yu Wen,² Chang Q Sun^{1,2*}

¹ *School of Electrical and Electronic Engineering, Nanyang Technological University, Singapore 639798*

³ *Faculty of Materials and Optoelectronic Physics, Xiangtan University, Hunan 411105, China*

***E-mail:** Ecqsun@ntu.edu.sg

With the aid of *ab initio* molecular dynamics calculations, we resolved the anomalies of frozen H₂O under compression such as the low compressibility and the pressure-induced Raman phonons shift and protons central symmetrization in the “O²⁻ : H^{+/p}-O²⁻” hydrogen-bond. We found that the initially longer-and-stiffer intermolecular “O²⁻ : H^{+/p}” nonbond is highly compressive and turns to be shorter and even stiffer but the shorter intramolecular “H^{+/p}-O²⁻” bond expands instead and becomes longer and weaker upon compression. Such transition happens because of the repulsion between the unevenly-bound electrons pairs. The practice and findings should shed light on the physical anomalies of H₂O.

I. Introduction

H₂O has been the subject of numerous investigations, given its paramount importance in the physical sciences¹⁻³ and its key role in DNA folding,^{4,5} protein and gene delivery.^{6,7} Although the structure formation and transition under pressures or cooling⁸⁻¹⁰ and the reaction dynamics¹¹ of H₂O have been intensively investigated, many fundamental questions about the properties of water away from ambient conditions are yet unanswered.¹²⁻¹⁶

For instances, it is usual that the crucial temperature (T_C) for liquid or disordered phase to transfer into solid or ordered phase increases with the pressure (P) in a quasi-equilibrium process.^{17,18} However, the T_C for Ice VIII phase transferring to proton-ordered Ice VII phase drops from 280K to 150K when the P increases from 1GPa to 50GPa.¹⁹ The melting temperature (T_m) of ice hexagonal phase also changes with P oppositely.^{20,21} Unlike other solid materials, the refractive index of ice increases and the band gap (E_G) drops when the P is elevated.²² These anomalies are beyond the expectation of Pauling's Ice Rule²³ that predicted the crystal geometry and entropy of various phases.

Intensive investigation has been conducted on the bond length and bond vibration of H₂O using Raman and Infrared spectroscopies under various conditions.^{19,24-26} O-O distances were found to change oppositely with O-H bond length, leading to the proton symmetrization of Ice VIII under high pressure.²⁷ Sun et al²⁴ decomposed the high-frequency Raman mode into components and attributed them to O-H vibrations engaged in different types of hydrogen bonding. Pruzan et al¹⁹ investigated the pressure and temperature effect on the Raman shift of both the low- and the high-frequency modes. The vibration spectra of ice-VIII measured by Raman scattering²⁵ and by infrared absorption²⁶ both demonstrated that the high-frequency mode shifts down while the low-frequency vibration mode shifts up when the applied pressure is increased. However, the correlation between the relaxation dynamics of the bond and the nonbond and the spectroscopic features as well as the observed anomalies of H₂O needs to be established.

II. Principles

An extension of Pauling's ice rule²³ (the central tetrahedron) and the principle of proton symmetrization under pressures are shown in **Error! Reference source not found.**, to contain two H₂O

molecules and four identical quasi-linear “O²⁻ : H^{+p}-O²⁻” hydrogen bonds.²⁸ The H^{+p} plays a dual role of H⁺ and H^p as it donates its electron to one O²⁻ and meanwhile it is polarized by the nonbonding lone pair of the other neighboring O²⁻ upon the sp-orbit of oxygen being hybridized in reaction.²⁹ In the hexagonal or cubic ice the O²⁻... O²⁻ distance is 0.276 nm. The intramolecular H^{+p}-O²⁻ bond is much shorter and stronger (~0.100 nm and ~10⁰ eV) than that of the intermolecular O²⁻ : H^{+p} nonbond (~0.176 nm and ~10⁻² eV). The angle between the H^{+p}-O²⁻-H^{+p} is smaller than 104.5° while the angle between the H^{+p} : O²⁻ : H^{+p} is greater than 108.5° for a free H₂O molecule. It has recently been confirmed³⁰ that the liquid water is consistent with a unimodel density of the tetrahedral structure at the ambient conditions.

The advantage of the extended Ice Rule is that it allows us to focus on one of the four “O²⁻ : H^{+p}-O²⁻” bonds to examine the responses of the intramolecular nonbonding lone pair “:” and the intermolecular bonding pair “-” of electrons to the applied stimulus and their correlation, for example, the proton symmetrization under pressure, as shown in Figure 1(b). The nonbonding lone pair “:” will be easier to be squeezed by pressures than the bonding pair “-”. When the ice is forced under pressures, the squeezed O²⁻ : H^{+p} nonbond will repulse the bonding pair “-” oppositely and hence the H^{+p}-O²⁻ bond will become longer, making the proton located in the middle of the O-O.

Under certain pressure and temperature, the correlation of bond length (d_x), bond energy (E_x), T_m and T_C can be expressed as,³¹

$$\begin{cases} \frac{E_x(P, T)}{E_x(P_0, T_0)} = 1 + \sum_J \Delta_J = C_x^{-m} + \frac{\int_{T_0}^T \eta(t) dt - \int_{V_0}^V p(v) dv}{E_x(P_0, T_0)} \\ T_m(P) \propto T_c(P) \propto E_-(P) \\ \text{with } C_x = \frac{d_x(P, T)}{d_x(P_0, T_0)} \end{cases} \quad (1)$$

where subscript x represents the “:” and “-”. Δ_J is the energy perturbation by the applied stimuli. $\eta(t)$ is the specific heat of the representative bond and m is the bond nature indicator which has values larger than 1. P_0 and T_0 are the taken as references. These expressions indicate that the compressive strain or mechanical hardening will strengthen the bond; but the thermal vibration or the tensile strain will

weaken the bond. T_m and T_C under different pressures are generally determined by the bonding strength of the O-H bond other than the O:H nonbonding pair. The generalized form indicates that we can consider all the stimuli either individually or collectively, depending on the experimental conditions.

The Raman spectroscopy could resolve the vibration of the intramolecular nonbond in the frequency range of $\omega_L < 300 \text{ cm}^{-1}$ and that of the intermolecular bond in the frequency range of $\omega_H > 3000 \text{ cm}^{-1}$. From the first order approximation and conventional approach for other existing materials,³² the bonding and nonbonding part of the hydrogen bond can be taken as a harmonic system with an interaction potential, $u(r_x)$. Equating the vibration energy of the harmonic system to the third term of the Taylor series of its interaction potential at equilibrium, we can obtain the relation:³¹

$$\begin{aligned} \frac{1}{2} \mu (\Delta \omega)^2 (r - d_x)^2 &\cong \frac{1}{2} \frac{\partial^2 u(r)}{\partial r^2} \bigg|_{r=d_x} x^2 \propto \frac{1}{2} \frac{E_x}{d_x^2} (r - d_x)^2 \\ \Delta \omega_x = \omega_x - \omega_{x0} &\propto \frac{E_x^{1/2}}{\mu d_x} \end{aligned} \quad (2)$$

Generally, the Raman shift depends on the length and energy of the bond and the reduced mass of the atom or molecule of the vibronic system. From the dimensional point of view, the second order derivative of the potential at equilibrium is proportional to the bind energy E_x divided by the bond length d_x^2 . The intrinsic vibration frequency is detectable as the Raman shift from the referential point ω_{x0} . This relation indicates that if the bond contracts or the binding energy increases, a blue shift will happen, and vice versa. Therefore, Raman frequency shift is supposed to tell us the change of the length and energy of the respective part of the hydrogen bond. This approach has been successfully used in analyzing the Raman shift of Si, C, and oxide materials, for which the bond energy is inversely proportional to a certain power of the bond length.^{31, 32}

Molecular dynamics (MD) calculations were performed using Forcite package with *ab initio* optimized force field Compass27.³³ The evolution of the O-H and O:H distances in a 32- molecules unit cell of ice-VIII under pressure from 1 to 20 GPa was dynamically relaxed in constant pressure, constant enthalpy (NPH) ensemble for 30ps. The O-H and O:H lengths were taken average of the structures of the last 10ps (20,000 steps). The power spectra were calculated from the Fourier transform of their

velocity autocorrelation function using velocity data of all atoms recorded at every 0.5 fs. The Fourier transform of the velocity autocorrelation function can be expressed as:³⁴

$$I(\omega) = F(\text{Cor}(t)) = 2 \int_0^\infty \text{Cor}(t) \cos \omega t dt$$

$$\text{With } \text{Cor}(t) = v(\tau) * v(-\tau) = \frac{\sum_{j=1}^{n_t} \sum_{i=1}^N v_i(\tau_j + t) v_i(\tau_j)}{\sum_{j=1}^{n_t} \sum_{i=1}^N v_i^2(\tau_j)}$$
(3)

Where v_i is the velocity of the i th atom and $*$ represents convolution. The velocities are taken from the last 10ps (20,000 steps).

III. Results

Table 1 lists and Figure 2(a) shows the length correlation between the $\text{O}^{2-} : \text{H}^{+/p}$ and the $\text{H}^{+/p} - \text{O}^{2-}$. When the pressure is increased from 1 to 20 GPa the $\text{H}^{+/p} : \text{O}^{2-}$ nonbond is compressed from 0.1767 to 0.1692 nm and meanwhile the $\text{H}^{+/p} - \text{O}^{2-}$ bond expands from 0.0974 to 0.1003 nm with a net linear compression of $\sim 1.7\%$. Combining the calculation results and Eq.(1), the relation between d_x and E_x of O-H or O:H bond can be expressed as:

$$\begin{cases} d_x = d_{x0}(1 + \alpha P + \beta P^2) \\ \frac{E_x(P)}{E_x(P_0)} = C_x^{-m} - \frac{\int_{d_{x0}}^{d_x} p(l_x) dl_x}{E_{x0}} \end{cases}$$
(4)

with the fitting parameters $d_{-0}=0.9732 \text{ \AA}$, $\alpha=8.940 \times 10^{-4}$, $\beta=2.896 \times 10^{-5}$; $d_{+0}=1.7687 \text{ \AA}$, $\alpha=-1.420 \times 10^{-4}$, $\beta=-1.028 \times 10^{-4}$. P_0 is taken as 0GPa. Figure 2(b) compares the calculated and measured pressure-dependent volume of iceVIII, with the fitting equation as $V/V_0 = 1 - 2.38 \times 10^{-2} P + 4.70 \times 10^{-4} P^2$. Figure 2(c) compares the T_c of iceVIII to proton-disordered phase iceVII determined by experiments^{19, 26, 35} with the theoretical P - T_c relation as expressed follows.

To perform the integration in Eq.(4) by substitution, we get

$$\int_{d_{x0}}^{d_x} p(l_x) dl_x = d_{x0} \int_{P_0}^P p \left(\frac{l_x}{d_{x0}} \right) \frac{dl_x}{d_{x0} dp} dp = d_{x0} \int_{P_0}^P p(\alpha + 2\beta p) dp$$

Thus, according to Eq. (1), T_c - P relation becomes

$$\frac{T_c(P)}{T_c(P_0)} = \frac{E_-(P)}{E_-(P_0)} = C_-^{-m} - \frac{d_{-0}}{E_{-0}} \left[\frac{\alpha(P^2 - P_0^2)}{2} + \frac{2\beta(P^3 - P_0^3)}{3} \right] \quad (5)$$

where $E_{-0}=5.2\text{eV}$ as O-H bond energy,³⁶ and $m=1$. Theoretical T_c - P curve agrees well with the experimental data, as shown in Figure 2(c).

The pressure dependence of the power spectra in the specified frequency ranges of $\omega_- < 400 \text{ cm}^{-1}$ and $\omega_+ > 3000 \text{ cm}^{-1}$, in Figure 3 (a), shows that as P increases, the ω_- shifts gradually from 3520 cm^{-1} to 3320 cm^{-1} and the ω_+ shifts from 336 to 120 cm^{-1} , disregarding the possible phase change and other supplementary peaks at ~ 300 and $\sim 3400 \text{ cm}^{-1}$. The measured vibration peaks of ω_- and ω_+ of ice-VIII measured at 80 K ²⁵, by Raman scattering study¹⁹, and by infra-red (IR) absorption study²⁶ are shown in Figure 3(b), compared with the calculated results. All the results are consistent to show that³¹ the enhancement of P causes the blue shift of the low-frequency mode and the red shift of the high-frequency stretching mode despite of the error caused by different investigation methods.

Therefore, we have to separate the binding energy and the bond length in Eq. (1) for H_2O with consideration of the effect of polarization and the screening effect.²⁸ Combining the MD-derived bond lengths and Raman spectral features, we are certain that as P increases, $\text{O}^{2-} : \text{H}^{+/p}$ is squeezed and becomes stronger but $\text{H}^{+/p} - \text{O}^{2-}$ bond is otherwise elongated and weakened, because of the polarization of the bonding electron by the shortened lone pair. Thus both the proton symmetrization and Raman features are incorporated and the pressure-induced T_c decrease is understood.

IV. Conclusion

Incorporating the MD-derived bond lengths and vibration information and the experimental results from Raman and IR spectra, it turns out that the initially longer and much weaker nonbond becomes shorter and stiffer and the initially shorter and stronger bond becomes longer and weaker upon pressure, which explains the proton symmetrization of hydrogen bond and the decrease of T_c , E_G , T_m of

ice under pressure. The transition happens because of the polarization and repulsion of the electrons by the nonbonding lone pair of the pressure-contracted nonbond that is in turn screened by the former. It is also found that the high-frequency “-” vibration dominates the physical and chemical properties of ice under pressure. Practice and findings may pave the path towards controlling the hydrogen-bond formation and relaxation dynamics and find applications in the hydrogen-bond involved species such as drug design, medication, signaling and messaging.

Table 1 MD derived lengths of the two parts and the resultant of the hydrogen bond of ice.

| P(GPa) | O-H (Å) | O:H (Å) | O-O(Å) |
|--------|---------|---------|---------|
| 1 | 0.97358 | 1.76708 | 2.74066 |
| 5 | 0.97901 | 1.76247 | 2.74148 |
| 10 | 0.98527 | 1.75041 | 2.73568 |
| 15 | 0.99125 | 1.72133 | 2.71258 |
| 20 | 1.00245 | 1.6919 | 2.69435 |

Figure 1 (a)An extension (2H₂O tetrahedron) of Pauling's "two-in two-out" ice rule (the central H₂O tetrahedron) allows us to focus on the cooperative interaction between the unevenly-bounded nonbonding lone pair ":" and bonding pair "-" of electrons in the quasi-linear "O²⁻: H^{+/p}-O²⁻" hydrogen bond. (b)The proton symmetrization of ice under pressures is induced by the squeezing of the nonbonding lone pair ":" and the oppositely compulsion of the bonding pair "-", making the proton located in the middle of O-O.

Figure 2(a) MD calculation results of pressure on the ":" or the "-" lengths. The O-O trend agrees with those reported in ³⁷⁻³⁹. Proton symmetrization occurring at 58.6GPa is realized by nonbonding pair compression and bonding pair expansion as pressure increases to, with O-O distance at about 2.21 Å; in accord with the experimental observations : 59GPa and 2.2 Å.²⁷ (b) Comparison of volume decay with pressure by calculation and experiment.⁴⁰(c)Phase transition temperature of iceVIII to proton-disordered iceVII in the phase diagram¹⁹ derived by experimental data1³⁵ and data2²⁶, compared with the theoretical P - T_c relation(black line).

Figure 3(a) MD derived power spectra of ice-VIII under pressure in comparison to (b) the measured vibration peaks of ω_- (circle) and ω_+ (square) of ice-VIII at 80 K ²⁵, by Raman scattering study¹⁹, and by infrared absorption study²⁶. The trends consistency evidences that ³¹ the compressed H^{+/p}: O²⁻ causes the blue shift of the low-frequency mode (100-400 cm⁻¹) and the elongated H^{+/p}-O²⁻ results in the red shift of the high-frequency stretching mode (3000-3500 cm⁻¹).

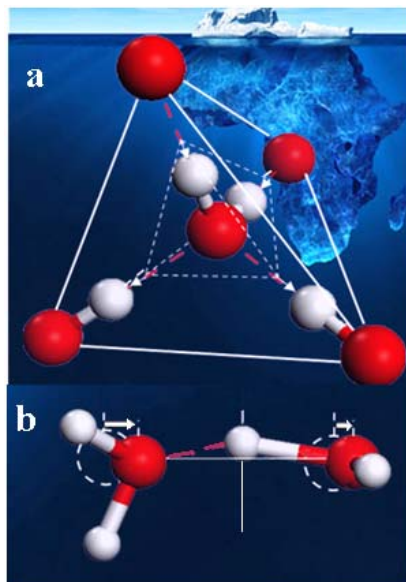


Figure 1

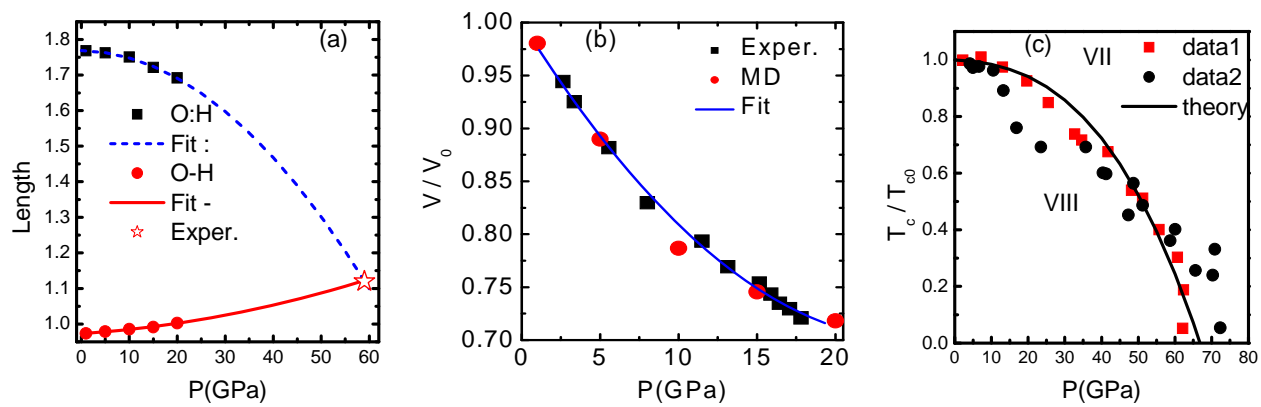


Figure 2

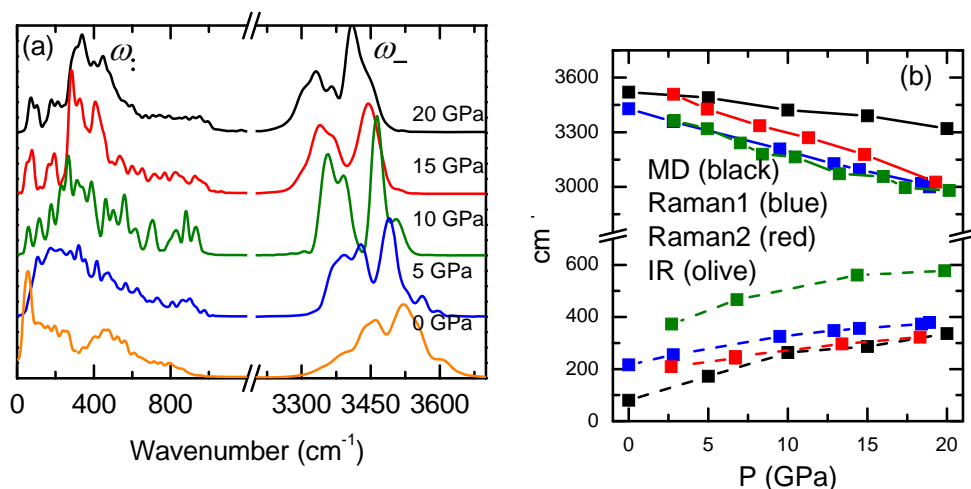


Figure 3

References

1. P. Ball, *Nature* **452** (7185), 291-292 (2008).
2. I. V. Stiopkin, C. Weeraman, P. A. Pieniazek, F. Y. Shalhout, J. L. Skinner and A. V. Benderskii, *Nature* **474** (7350), 192-195 (2011).
3. D. Marx, M. E. Tuckerman, J. Hutter and M. Parrinello, *Nature* **397** (6720), 601-604 (1999).
4. M. Smyth and J. Kohanoff, *Phys. Rev. Lett.* **106** (23), 238108 (2011).
5. P. Baaske, S. Duhr and D. Braun, *Appl. Phys. Lett.* **91** (13), 133901 (2007).
6. C. Castellano, J. Generosi, A. Congiu and R. Cantelli, *Appl. Phys. Lett.* **89** (23), 233905 (2006).
7. J. H. Park and N. R. Aluru, *Appl. Phys. Lett.* **96** (12), 123703 (2010).
8. K. Kobayashi, M. Koshino and K. Suenaga, *Phys. Rev. Lett.* **106** (20), 206101 (2011).
9. A. Hermann and P. Schwerdtfeger, *Phys. Rev. Lett.* **106** (18), 187403 (2011).
10. W. Chen, X. F. Wu and R. Car, *Phys. Rev. Lett.* **105** (1), 017802 (2010).
11. C. K. Lin, C. C. Wu, Y. S. Wang, Y. T. Lee, H. C. Chang, J. L. Kuo and M. L. Klein, *PCCP* **7** (5), 938-944 (2005).
12. J. W. M. Frenken and T. H. Oosterkamp, *Nature* **464** (7285), 38-39 (2010).
13. J. M. Headrick, E. G. Diken, R. S. Walters, N. I. Hammer, R. A. Christie, J. Cui, E. M. Myshakin, M. A. Duncan, M. A. Johnson and K. D. Jordan, *Science* **308** (5729), 1765-1769 (2005).
14. J. K. Gregory, D. C. Clary, K. Liu, M. G. Brown and R. J. Saykally, *Science* **275** (5301), 814-817 (1997).
15. N. Bjerrum, *Science* **115** (2989), 385-390 (1952).
16. A. K. Soper, J. Teixeira and T. Head-Gordon, *Proceedings of the National Academy of Sciences of the United States of America* **107** (12), E44-E44 (2010).
17. C. Q. Sun, *Prog. Mater. Sci.* **54** (2), 179-307 (2009).
18. D. Errandonea, B. Schwager, R. Ditz, C. Gessmann, R. Boehler and M. Ross, *Phys. Rev. B* **63** (13), 132104 (2001).
19. P. P. J. C. Chervin, E. Wolanin, B. Canny, M. Gauthier and M. Hanfland, *J. Raman Spectrosc.* **34**, 591-610 (2003).
20. G. M. Marion and S. D. Jakubowski, *Cold Regions Science and Technology* **38** (2-3), 211-218

- (2004).
21. E. Schwegler, M. Sharma, F. Gygi and G. Galli, Proceedings of the National Academy of Sciences of the United States of America **105** (39), 14779-14783 (2008).
 22. C. S. Zha, R. J. Hemley, S. A. Gramsch, H. K. Mao and W. A. Bassett, J. Chem. Phys. **126** (7), 074506 (2007).
 23. L. Pauling, J. Am. Chem. Soc. **57**, 2680-2684 (1935).
 24. Q. Sun and H. Zheng, Progress in Natural Science **19** (11), 1651-1654 (2009).
 25. Y. Yoshimura, S. T. Stewart, M. Somayazulu, H. Mao and R. J. Hemley, J. Chem. Phys. **124** (2), 024502 (2006).
 26. M. Song, H. Yamawaki, H. Fujihisa, M. Sakashita and K. Aoki, Physical Review B **60** (18), 12644 (1999).
 27. M. Benoit, D. Marx and M. Parrinello, Nature **392** (6673), 258-261 (1998).
 28. C. Q. Sun, Nanoscale **2** (10), 1930-1961 (2010).
 29. C. Q. Sun, Prog. Mater. Sci. **48** (6), 521-685 (2003).
 30. G. N. I. Clark, G. L. Hura, J. Teixeira, A. K. Soper and T. Head-Gordon, Proceedings of the National Academy of Sciences of the United States of America **107** (32), 14003-14007 (2010).
 31. C. Q. Sun, Prog. Solid State Chem. **35** (1), 1-159 (2007).
 32. X. X. Yang, J. W. Li, Z. F. Zhou, Y. Wang, W. T. Zheng and C. Q. Sun, Appl Phys Lett **DOI: 10.1063/1.3645015** (2011).
 33. H. Sun, J. Phys. Chem. B **102**, 7338 (1998).
 34. J. Wang, Q. H. Qin, Y. L. Kang, X. Q. Li and Q. Q. Rong, Mech. Mater. **42** (5), 537-547 (2010).
 35. K. Aoki, H. Yamawaki and M. Sakashita, Physical Review Letters **76** (5), 784 (1996).
 36. A. D. McNaught and A. Wilkinson, *IUPAC. Compendium of Chemical Terminology*, 2nd ed. (Blackwell Scientific Publications, Oxford, 1997).
 37. K. Liu, J. D. Cruzan and R. J. Saykally, Science **271** (5251), 929-933 (1996).
 38. R. Ludwig, Angewandte Chemie-International Edition **40** (10), 1808-1827 (2001).
 39. D. Kang, J. Dai, Y. Hou and J. Yuan, *Structure and vibrational spectra of small water clusters from first principles simulations*. (AIP, 2010).
 40. Y. Yoshimura, S. T. Stewart, M. Somayazulu, H. Mao and R. J. Hemley, Journal of Chemical Physics **124** (2) (2006).